Computational algorithm for geometrically nonlinear analysis of laminated composite frames with zig-zag enhancement of the transverse strain field

Caio C. L. G. Bernardo[1], Humberto B. Coda[1], Rodrigo R. Paccola[1]

1_Dept. of Structural Engineering, São Carlos School of Engineering, University of São Paulo_
Av. Trab. São Carlense, 400, 13566-590, São Carlos, São Paulo, Brazil
caiolacava@usp.br, hbcoda@sc.usp.br, rpaccola@sc.usp.br

Abstract. Laminated composite materials are widely used in engineering applications due to the high control and flexibility over the design of its mechanical properties. It is known, however, that when subjected to loads, structural elements made of laminated composites display a zig-zag pattern on their strain field in the transverse direction, behaving differently from the usual assumption that considers transverse sections as planes after the load application for calculation purposes. Therefore, this work proposes the implementation of a finite element method computational algorithm, based on positions, that numerically solves laminated composite frames by enhancing the strain field in the transverse direction. The first order shear deformation theory (FSDT) adapted for generalized vectors is used as the basic kinematic assumption, and then enhanced by a normalized zig-zag-shaped function multiplied by an amplitude factor, which is a new nodal degree of freedom. In addition, the cross section direction and height variation are represented by generalized vectors, which are also nodal degrees of freedom. The developed formulation is total Lagrangian, comprising large displacements and rotations, and uses the Saint-Venant-Kirchhoff constitutive law, which allows moderate strains.

Keywords: Zig-zag enhancement, Geometrically nonlinear analysis, Positional FEM, Laminated composites.

1   Introduction

During the development of engineering technologies, the need for materials with specific properties became usual. However, some of these properties may not be obtained from pure materials in nature. For that reason, different components were combined on a macroscopic scale to create new materials with specific characteristics to supply its design task. This process originates unique materials known as composites. According to Jones [1], if the composite material is well designed, it can display not only the best property of its constituents, but also unique properties that they do not exhibit apart. Some of the characteristics that can be enhanced are strength, stiffness, weight, fatigue live, thermal insulation, thermal conductivity, wear resistance and corrosion resistance.

Laminated composites, as stated by Jones [1], are widely used in the industry due to its capability of owning high strength-to-weight and stiffness-to-weight ratios. As the name suggests, they are made of different layers stacked and bonded together. Reddy [2] explains that a layer, also known as lamina or ply, is a sheet of material that can be described as a fundamental building block for the laminate. As a result, this type of composite presents different properties along the transverse direction, which leads to an effect in the in-plane displacement field known as zig-zag.

There are many theories to predict the mechanical behavior of laminated composite structures. According to Carrera [3], Carrera and Ciuffreda [4] and Sayyad and Ghugal [5], the equivalent single-layer theories (ESL) usually work fine for global behavior and require less computation effort than other theories. However, they cannot exhibit the zig-zag kinematic and display discontinuous transverse stresses. Some researches like Meunier and Shenoi [6], Liu and Paavola [7] and Wang et al. [8] are examples of ESL implementation. Carrera [3] and Carrera and Ciuffreda [4] mention that the layerwise theories (LW), on the other hand, can model the

zig-zag effect at the cost of more computation effort. That happens because each layer is modeled independently and the number of unknowns increases with the number of layers. According to Sayyad and Ghugal [5], its results are usually close to the three-dimensional elasticity solutions. Some examples of layerwise theories application can be found at Robbins and Reddy [9] and Tahani [10].

As an alternative, Coda et al. [11] proposed a positional formulation for laminated plates and shells with generalized vectors to model the transverse lines direction. The formulation uses a kinematic similar to the Reissner-Mindlin one (ELS), but it is enhanced by a precomputed constant zig-zag profile and has transverse stress regularization.

As an improvement of the work presented by Coda et al. [11], this paper presents a positional formulation that includes the zig-zag effect as a nodal degree of freedom for 2D laminated composite frames, including this behavior in the energy minimization process. The presented formulation is a geometrically nonlinear total Lagrangian approach and uses the Saint Venant-Kirchhoff constitutive law, which allows moderate strains. It is a promising strategy from which the stress regularization and the generalization to shell applications are the next research goal.

2 Formulation

The presented positional formulation uses positions and generalized vectors as nodal unknowns instead of displacements and rotations. In derivations the layers are perfectly attached to each other, the strains are small, each layer is perfectly homogeneous, the thickness of each layer is constant throughout the element in the initial configuration, the cross sections are rectangular and the external forces are conservative.

2.1 Mapping and deformation function

The reference line of frame elements is approached by third order Lagrange polynomial interpolation and is positioned at the stiffness center of the laminate. Any point in a specific element layer can be found at the non-deformed configuration by the following mapping function:

$$f_i^{0k}\left(\xi_1, \xi_2^{(k)}\right) = x_i^k = \phi_\ell(\xi_1)X_i^\ell + \left(\frac{h_k}{2}\xi_2^{(k)} + \bar{x}_k - \bar{x}_{cg}\right)\phi_\ell(\xi_1)V_i^\ell, \tag{1}$$

where f_i^{0k} is the i-th coordinate of the initial mapping function for layer k, x_i^k is the i-th coordinate of the initial position of a point in layer k, X_i^ℓ is the i-th initial coordinate of the reference line node ℓ, h_k is the initial thickness of layer k, $\bar{x}_k$ is the distance between the cross section bottom surface and the center of the k-th layer, $\bar{x}_{cg}$ is the coordinate of the cross section stiffness center measured from its bottom surface, V_i^ℓ is the coordinate i of the node ℓ initial generalized vector, ξ_1 and ξ_2^k are the dimensionless coordinates from the isoparametric domain and ϕ_ℓ is the shape function related to node ℓ.

Like eq. (1), there is another mapping function related to the current configuration of the structure. To make it simpler, the sum of the three terms in eq. (1) inside the parentheses will be called $\eta^k\left(\xi_2^{(k)}\right)$. Thus, the current configuration mapping function can be written as:

$$\begin{aligned} f_i^{1k}\left(\xi_1, \xi_2^{(k)}\right) = y_i^k = \phi_\ell(\xi_1)Y_i^\ell + \left[\eta^k\left(\xi_2^{(k)}\right) + \phi_\ell(\xi_1)\bar{T}^\ell \cdot \eta^k\left(\xi_2^{(k)}\right)^2\right]\phi_\ell(\xi_1)G_i^\ell \\ +\phi_\ell Z^\ell\left(a_k\xi_2^{(k)} + \ell_k\right)(-1)^{i+1}\phi_j G_{3-(i)}^j, \end{aligned} \tag{2}$$

where f_i^{1k} is the i-th coordinate of the current mapping function for layer k, y_i^k is the i-th coordinate of the current position of a point in layer k, Y_i^ℓ is the i-th current coordinate of the reference line node ℓ, $\bar{T}^\ell$ is a nodal parameter to introduce linear behavior to the transverse strain in order to avoid volumetric locking as studied by Bischoff and Ramm [12], G_i^ℓ is the coordinate i of the current generalized vector related to node ℓ, Z^ℓ is the magnitude of the zig-zag enhancement profile at node ℓ and $(a_k\xi_2^{(k)} + \ell_k)$ is the normalized zig-zag profile. It is important to note that the last term of eq. (2) is the original contribution of this work.

Relying on eq. (1) and eq. (2), the deformation function can be expressed as:

$$\vec{f}(x_1, x_2) = \vec{f}^1\left(\vec{f}^{0^{-1}}(x_1, x_2)\right), \tag{3}$$

and Fig. 1 displays the deformation and mapping process of a finite element.
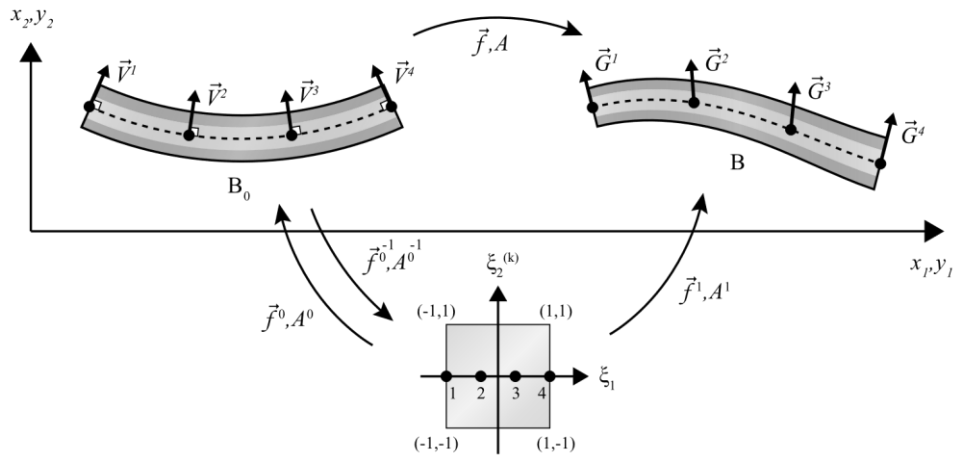
Figure 1. Deformation and mapping functions

The gradient of the deformation function $\boldsymbol{A}$ can be written, considering eq. (3), as:

$$\boldsymbol{A} = \boldsymbol{A}^1 \cdot (\boldsymbol{A}^0)^{-1}, \tag{4}$$

where

$$A_{ij}^0 = \frac{\partial f_i^0}{\partial \xi_j} \quad \text{and} \quad A_{ij}^1 = \frac{\partial f_i^1}{\partial \xi_j}. \tag{5}$$

2.2 Zig-zag enhancement profile

The zig-zag enhancement profile is composed by line segments defined by layer. Each layer has 2 unknowns: a_k and ℓ_k. To determine them, however, the expression $a_k \xi_2^{(k)} + \ell_k$ is first converted to $a_k \bar{x} + b_k$, where $\bar{x}$ is the height of a point measured from the cross section bottom surface. Therefore, a_k and b_k are calculated and then converted back to a_k and ℓ_k. If the laminate has n layers, $2n$ equations are needed.

The first $n - 1$ equations impose continuity between adjacent layers:

$$a_k \left(\bar{x}_k + \frac{h_k}{2} \right) + b_k = a_{k+1} \left(\bar{x}_k + \frac{h_k}{2} \right) + b_{k+1}, \quad 1 \le k \le n - 1. \tag{6}$$

Furthermore, it is assumed that the zig-zag profile does not generate normal force or bending moment resultants. In these circumstances and knowing that the profile is qualitative only, two equilibrium equations can be written:

$$\sum_{k=1}^n \int_{h_k} (a_k \bar{x} + b_k) \mathbb{E}^k d\bar{x} = 0, \tag{7}$$

$$\sum_{k=1}^n \int_{h_k} \bar{x}(a_k \bar{x} + b_k) \mathbb{E}^k d\bar{x} = 0, \tag{8}$$

where $\mathbb{E}^k$ is the Young's modulus of the k-th layer.

Finally, the last $n - 1$ equations are obtained from the relationship between slopes of adjacent layers. This expression was suggested by Coda et al. [11] after observing analytical solutions available in literature:

$$a_k - a_{k+1} = \frac{\mathbb{E}^k h_{(k)}^3 - \mathbb{E}^{k+1} h_{(k+1)}^3}{\left(\bar{x}_k + \frac{h_k}{2} - \bar{x}_{cg}\right)\left(\mathbb{E}^k h_{(k)}^3 + \mathbb{E}^{k+1} h_{(k+1)}^3\right)}, \qquad 1 \le k \le n-1. \tag{9}$$

Thus, the constants a_k and b_k can be converted back to a_k and $\mathcal{b}_k$ using the following equations:

$$a_k = \frac{a_k h_{(k)}}{2} \quad \text{and} \quad \mathcal{b}_k = a_k \bar{x}_{(k)} + b_k. \tag{10}$$

2.3 Equilibrium equations

In this research, the equilibrium equations are achieved by the Principle of Stationary Mechanical Energy. The total mechanical energy Π is the sum of the total strain energy $\mathbb{U}$, the potential energy of external forces $\mathbb{P}$ and the kinetic energy $\mathbb{K}$. As this work focuses only on static analysis, the kinetic energy term is not considered. In that perspective, the equilibrium occurs when:

$$\delta\Pi = \delta\mathbb{U} + \delta\mathbb{P} = \left(\frac{\partial\mathbb{U}}{\partial\vec{Y}} + \frac{\partial\mathbb{P}}{\partial\vec{Y}}\right)\delta\vec{Y} = 0 \therefore \frac{\partial\Pi}{\partial\vec{Y}} = \frac{\partial\mathbb{U}}{\partial\vec{Y}} + \frac{\partial\mathbb{P}}{\partial\vec{Y}} = \vec{0}, \tag{11}$$

where $\vec{Y}$ is a vector with all the nodal parameters.

The total strain energy $\mathbb{U}$ and its derivative with respect to $\vec{Y}$ are, respectively:

$$\mathbb{U} = \int_{V_0} u_e dV_0, \tag{12}$$

$$\frac{\partial\mathbb{U}}{\partial\vec{Y}} = \int_{V_0} \frac{\partial u_e}{\partial\vec{Y}} dV_0 = \int_{V_0} \frac{\partial u_e}{\partial\boldsymbol{E}} : \frac{\partial\boldsymbol{E}}{\partial\vec{Y}} dV_0 = \int_{V_0} \boldsymbol{S} : \frac{\partial\boldsymbol{E}}{\partial\vec{Y}} dV_0, \tag{13}$$

in which $\boldsymbol{E}$ is the Green-Lagrange strain tensor, $\boldsymbol{S}$ is the second Piola-Kirchhoff stress tensor and u_e is the strain energy density function of the constitutive model used. The Green-Lagrange strain tensor is defined by:

$$\boldsymbol{E} = \frac{1}{2}(\boldsymbol{A}^t\boldsymbol{A} - \boldsymbol{I}), \tag{14}$$

where $\boldsymbol{I}$ is the identity matrix. The Saint Venant-Kirchhoff constitutive model is adopted. Its strain energy density function and the associated second Piola-Kirchhoff stress tensor are defined, respectively, by:

$$u_e^{SVK} = \frac{1}{2}\boldsymbol{E} : \mathfrak{C} : \boldsymbol{E}, \tag{15}$$

$$\boldsymbol{S}^{SVK} = \mathfrak{C} : \boldsymbol{E}, \tag{16}$$

in which $\mathfrak{C}$ is the constitutive tensor that is the same as the one used in Hooke's law.

The potential energy of the external conservative forces and its derivative with respect to current nodal positions Y_i^ℓ are, respectively:

$$\mathbb{P} = -F_i^\ell Y_i^\ell - \int_{-1}^{1} \left(\phi_j(\xi_1)Q_i^j\right)\left(\phi_\ell(\xi_1)Y_i^\ell\right)J_0^m(\xi_1)d\xi_1, \tag{17}$$

$$\frac{\partial\mathbb{P}}{\partial Y_i^\ell} = -F_i^\ell - \int_{-1}^{1} \left(\phi_j(\xi_1)Q_i^j\right)\phi_\ell(\xi_1)J_0^m(\xi_1)d\xi_1, \tag{18}$$

where Q_i^j is the coordinate i of the load per unit of length at node j. J_0^m is the Jacobian determinant defined by:

$$J_0^m = \sqrt{x_{1,\xi_1}^2 + x_{2,\xi_1}^2}. \tag{19}$$

2.4 Solution of nonlinear equations

The system of equations obtained from eq. (11) is nonlinear with respect to nodal parameters $\vec{Y}$. To solve it, the Newton-Raphson iterative method is used, defined by:

$$\left. \frac{\partial \vec{g}(\vec{Y})}{\partial \vec{Y}} \right|_{Y_t} \Delta Y_t = -\vec{g}(\vec{Y}_t) \quad \text{and} \quad \vec{Y}_{t+1} = \vec{Y}_t + \Delta \vec{Y}_t, \tag{20}$$

where:

$$\vec{g}(\vec{Y}) = \frac{\partial \Pi(\vec{Y})}{\partial \vec{Y}} \quad \text{and} \quad \frac{\partial \vec{g}(\vec{Y})}{\partial \vec{Y}} = \frac{\partial^2 \mathbb{U}}{\partial \vec{Y} \otimes \partial \vec{Y}} = \int_{V_0} \left(\frac{\partial \boldsymbol{S}}{\partial \vec{Y}} : \frac{\partial \boldsymbol{E}}{\partial \vec{Y}} + \boldsymbol{S} : \frac{\partial^2 \boldsymbol{E}}{(\partial \vec{Y} \otimes \partial \vec{Y})} \right) dV_0 = \boldsymbol{H}. \tag{21}$$

The initial nodal positions and generalized vectors are used as a first solution attempt for these parameters. For the kinematic enhancement $\bar{T}$ and Z, zero is the first attempt. With respect to integrations, the Gauss-Legendre quadrature is used. In addition, the chosen stopping criteria for the iterations, given a tolerance tol, is:

$$\frac{|\Delta \vec{Y}|}{|\vec{Y}_0|} < tol. \tag{22}$$

After achieving the current parameters, the second Piola-Kirchhoff stress tensor $\boldsymbol{S}$ can be transformed to the Cauchy stress tensor $\boldsymbol{\sigma}$ by the following relation:

$$\boldsymbol{\sigma} = \frac{1}{det(\boldsymbol{A})} \boldsymbol{A} \cdot \boldsymbol{S} \cdot \boldsymbol{A}^t. \tag{23}$$

3   Numeric example

In order to validate the algorithm implemented so far, the first example in Coda et al. [11] was reproduced. It is about a clamped beam with a total height of h composed by three layers perfectly attached and subjected to a uniform transverse load q, as shown in Fig. 2. There are two variations of this example with three cases each: (1) $q = 1.0 \times 10^{-3} \ kN/cm^2$ and $h = 60 \ cm$ and (2) $q = 1.0 \times 10^{-6} \ kN/cm^2$ and $h = 6 \ cm$. The three cases are the ply arrangements of the laminate, from the lower layer to the upper layer: (a) $\mathbb{E}_1$, $\mathbb{E}_2$, $\mathbb{E}_1$, (b) $\mathbb{E}_2$, $\mathbb{E}_1$, $\mathbb{E}_2$ and (c) $\mathbb{E}_2$, $\mathbb{E}_1$, $\mathbb{E}_1$, in which $\mathbb{E}_1 = 100 \ kN/cm^2$ and $\mathbb{E}_2 = 5 \ kN/cm^2$. Moreover, zero Poisson was assumed for all layers.

Coda et al. [11] processed the example with seven distinct kinematics, but only two were selected here for comparison: TB, which is the Euler-Bernoulli kinematics improved with the shear force contribution and 7PN, which has the enhanced kinematic without regularization of the transverse stresses. Similarly, the example was processed for this paper with two different kinematics: TZ0, which is the kinematic from eq. (1) and eq. (2) with $\bar{T}$ and Z parameters restricted and equal to zero, and TZ1, which is the kinematic with $\bar{T}$ and Z parameters unrestricted.

The beam was modeled by three finite elements with equally spaced nodes and the iteration tolerance used was 10^{-7}. The vertical displacement at the free edge obtained by this work and by Coda et al. [11] can be seen in Tab. 1 for all the six cases.
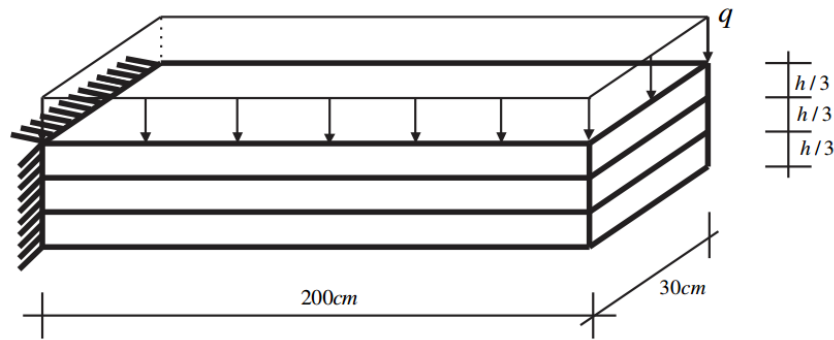
Figure 2. Geometrical parameters and boundary conditions. Source: Coda et al. [11]

Table 1. Vertical displacement at the free edge of the example for each case and kinematic

Case	TZ0 (cm)	TZ1 (cm)	TB (cm)	7PN (cm)
1a	0.1249	0.1258	0.1220	0.1262
1b	1.3225	1.3227	1.3160	1.3228
1c	0.3301	0.3308	0.2960	0.3303
2a	0.1153	0.1153	0.1157	0.1153
2b	1.3045	1.3045	1.3045	1.3045
2c	0.3204	0.3204	0.2897	0.3203

As one can see in Tab. 1, the displacements obtained by this work are very close to the one with 7PN kinematic calculated by Coda et al. [11]. The addition of $\bar{T}$ and Z parameters made the structure more flexible. In addition, the transverse stress profile at the support is displayed in Fig. 3 for case 1a for both TZ0 and TZ1 kinematics, where directions 1 and 2 are the longitudinal and transverse directions, respectively.
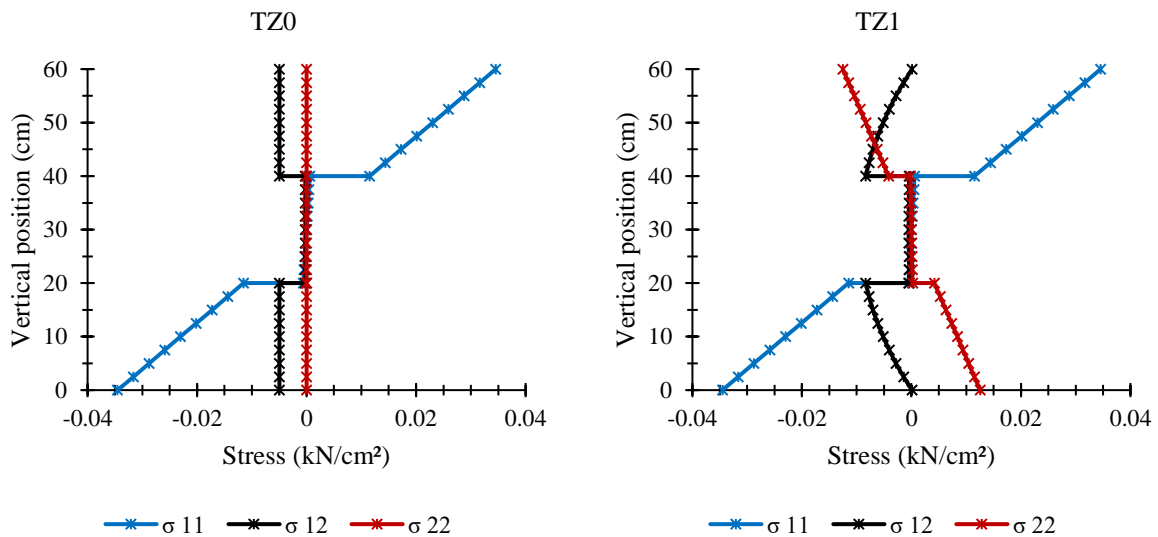
Figure 3. Vertical stress profile at the support for case 1a for kinematics TZ0 and TZ1

As can be seen, the shear stress (σ_{12}) for kinematic TZ0 is constant for each layer. In contrast, the shear stress distribution for kinematic TZ1, although still discontinuous between layers, already displays a quadratic behavior and homogeneous conditions on both free surfaces.

4   Conclusions

The formulation implemented so far revealed to be effective for geometrically nonlinear analysis of laminated frames. The displacements obtained agree with the ones selected in the literature and the transverse shear stress profile not only behaves quadratically but also exhibit homogeneous conditions on both free surfaces. The next steps of the research include: the stress regularization, generalization for plates and shells applications and plasticity with the zig-zag enhancement profile being updated as the plasticity develops.

Authorship statement. The authors hereby confirm that they are the sole liable persons responsible for the authorship of this work, and that all material that has been herein included as part of the present paper is either the property (and authorship) of the authors, or has the permission of the owners to be included here.

References

[1] Jones, R. M., 1999. *Mechanics of composite materials*. Taylor & Francis, Philadelphia, PA, 2nd ed edition.
[2] Reddy, J. N., 2004. *Mechanics of laminated composite plates and shells: theory and analysis*. CRC Press, Boca Raton, 2nd ed edition.
[3] Carrera, E., 2002. Theories and finite elements for multilayered, anisotropic, composite plates and shells. *Archives of Computational Methods in Engineering*, vol. 9, n. 2, pp. 87–140.
[4] Carrera, E. & Ciuffreda, A., 2005. A unified formulation to assess theories of multilayered plates for various bending problems. *Composite Structures*, vol. 69, n. 3, pp. 271–293.
[5] Sayyad, A. S. & Ghugal, Y. M., 2017. Bending, buckling and free vibration of laminated composite and sandwich beams: A critical review of literature. *Composite Structures*, vol. 171, pp. 486–504.
[6] Meunier, M. & Shenoi, R., 2001. Dynamic analysis of composite sandwich plates with damping modelled using high-order shear deformation theory. *Composite Structures*, vol. 54, n. 2-3, pp. 243–254.
[7] Liu, Q. & Paavola, J., 2018. General analytical sensitivity analysis of composite laminated plates and shells for classical and first-order shear deformation theories. *Composite Structures*, vol. 183, pp. 21–34.
[8] Wang, Y., Ren, H., Fu, T., & Shi, C., 2020. Hygrothermal mechanical behaviors of axially functionally graded microbeams using a refined first order shear deformation theory. *Acta Astronautica*, vol. 166, pp. 306–316.
[9] Robbins, D. H. & Reddy, J. N., 1993. Modelling of thick composites using a layerwise laminate theory. *International Journal for Numerical Methods in Engineering*, vol. 36, n. 4, pp. 655–677.
[10] Tahani, M., 2007. Analysis of laminated composite beams using layerwise displacement theories. *Composite Structures*, vol. 79, n. 4, pp. 535–547.
[11] Coda, H. B., Paccola, R. R., & Carrazedo, R., 2017. Zig-Zag effect without degrees of freedom in linear and non linear analysis of laminated plates and shells. *Composite Structures*, vol. 161, pp. 32–50.
[12] Bischoff, M. & Ramm, E., 1997. Shear deformable shell elements for large strains and rotations. *International Journal for Numerical Methods in Engineering*, vol. 40, n. 23, pp. 4427–4449.